EFFECT OF PLASTIC DEFORMATION AT ROOM TEMPERATURE ON HYDROGEN DIFFUSION OF HOT-ROLLED S30408

Wenmin Qu[1], Chaohua Gu[2], Jinyang Zheng[3]*, Yongzhi Zhao[4] and Zhengli Hua [5]
[1] Department of Energy Engineering, Zhejiang University, Institute of Process Equipment, Zheda Rd. No. 38, Hangzhou, 310027, PR China, wenminqu@zju.edu.cn
[2] Department of Energy Engineering, Zhejiang University, Institute of Process Equipment, Zheda Rd. No. 38, Hangzhou, 310027, PR China, guchaohua@zju.edu.cn
[3] Department of Energy Engineering, Zhejiang University, Institute of Process Equipment, Zheda Rd. No. 38, Hangzhou, 310027, PR China, jyzh@zju.edu.cn
[4] Department of Energy Engineering, Zhejiang University, Institute of Process Equipment, Zheda Rd. No. 38, Hangzhou, 310027, PR China, yzzhao@zju.edu.cn
[5] Department of Energy Engineering, Zhejiang University, Institute of Process Equipment, Zheda Rd. No. 38, Hangzhou, 310027, PR China, huazhengli007@126.com

ABSTACT

The influence of plastic deformation on hydrogen diffusion is of critical significance for hydrogen embrittlement (HE) studies. In this work, thermal desorption spectroscope (TDS), slow strain rate test (SSRT), feritscope, transmission electron microscope (TEM) and TDS model are used to establish the relationship between plastic deformation and hydrogen diffusion, aiming at unambiguously elucidating the effect of pre-existing traps on hydrogen diffusion of hot-rolled S30408. An effective way is developed to deduce hydrogen apparent diffusivity in this paper. Results indicate apparent diffusivities decrease firstly and then increase with increasing plastic strain at room temperature. Hydrogen diffusion changing with plastic deformation is a complicated process involving multiple factors. It is suggested to be divided into two processes controlled by dislocations and strain-induced martensite, respectively, and the transformation strain is about 20% demonstrated by experiments.

Keywords: hot-rolled S30408; hydrogen embrittlement; hydrogen diffusion; plastic deformation; TDS; apparent diffusivity; microstructures

NOMENCLATURE

C_L	concentration of hydrogen in the normal iron crystal lattice
t	time, s
$2d$	thickness of the plate specimen, m
D_e	effective diffusivity, m^2/s
C_{tot}	total concentration of hydrogen
C_0	hydrogen equilibrium concentration in the crystal lattice under hydrogen atmosphere
D_L	diffusivity in crystal lattice, m^2/s
γ	a constant value
C_T	trap density, $/m^2$
E_b	binding energy between hydrogen and the specific trap, J/mol
R	universal gas constant, J/(mol K)
T	temperature, K
C_x	concentration of the trapped hydrogen
D_{0L}	prefactor of diffusion, m^2/s
E_{diff}	active energy of diffusion, J/mol
E_t	activation energy for hydrogen to jump into the specific trap, J/mol
E_a	activation energy for hydrogen desorption from the specific trap, J/mol

1.0 INTRODUCTION

Hydrogen diffusion affected by plastic deformation serves as an important precondition of hydrogen embrittlement (HE) research. Pre-existing hydrogen traps can be introduced into materials inevitably during processing, strain strengthening, etc [1, 2] and have a significant effect on the diffusion

behavior of hydrogen in the material, resulting in hydrogen-assisted fracture. Austenitic stainless steels are commonly employed in valve bodies, pressure vessels and pipelines in hydrogen environment for their corrosion resistance, low ductile-brittle transition temperature, high toughness and ductility, etc [3]. However, hydrogen diffusivities lack consistency somewhat in austenitic stainless steels, especially when considering the effect of plastic deformation [4-10]. Therefore, it is necessary to measure the true hydrogen diffusivities, understand hydrogen diffusion rules, clarify the root causes of the effect of pre-existing traps on it in austenitic stainless steels when they are subjected to plastic deformation.

Hydrogen diffusion influenced by plastic deformation has been discussed in previous studies. Louthan et al. [11], And et al. [12] and Oriani et al. [13] have suggested that plastic deformation affect dislocation densities, induce martensite transformation and influence behaviours of grain boundary. Hydrogen segregates at and interacts with hydrogen traps, which results in crack initiation from there. α'-martensite is apt to be transformed from austenite directly or through precursor of ε-martensite and dislocation pile-ups in metastable austenitic stainless steels during plastic deformation because of a lower stability [14-20]. Compared to austenite, martensite can increase the rate of work-hardening and is conducive to formability. However, B. Ladna and H. K. Birnbaum [21] investigated hydrogen diffusion in type 304 stainless steel electrochemically charged with $^{2}H(D)$ in 1N D_2SO_4 with 0.25 g/l $NaAsO_2$ during 5%-8.5% strain. And the results manifests strain-induced martensite increases the penetration depth of the deuterium and acts as a rapid diffusion path owing to the considerably difference of diffusivity and solubility between α'-martensite and γ-austenite [22, 23], which accelerates the initiation and development of HE [24-27]. For hydrogen transport by dislocation, John K. Tien et al. [28] have proposed a kinetic model for hydrogen diffusion called dislocation sweep-in model which considers the increasing localized hydrogen concentration results from hydrogen diffusion by dislocation. Conversely, Kurkela et al. [29] and Donowan et al. [30] carried out experiments and did not support sweep-in model mentioned above. B. LADNA et al. [21] investigated the effect of plastic deformation on the diffusion of D into Ni, 310 SS, 304 SS from a cathodically charged surface using SIMS techniques. The results manifestes that dislocation transport of D did not make a significant contribution to diffusion under the conditions for which transport of D atmospheres. From above, one can conclude hydrogen diffusion changing with plastic deformation is unsettled and there is no consensus on the impact of hydrogen traps.

Currently, electrochemical permeation technique (EPT) is most commonly employed for measuring hydrogen permeability, including diffusivity and solubility [4, 31-33]. However, this method is restricted to a lower temperature. Thus, it is inappropriate to austenite stainless steels due to a lower hydrogen diffusivity of austenite stainless steels [33-35]. Furthermore, electrochemical charging may bring about some problems, such as corrosion and martensite transformation owing to the compressive stress on surface [36]. Sequentially, this method affects surface and inner microstructures of materials. Therefore, it acts as a crux to develop an effective and general method to deduce hydrogen diffusivity, which serves as the foundation for hydrogen diffusion studies.

In this work, SSRT, TDS, feritscope, TEM and TDS model are performed to investigate the effect of plastic deformation at room temperature on hydrogen diffusion of hot-rolled S30408. The results and discussions are outlined with three sections to start on. First, an effective method is developed to deduce apparent diffusivity based on the holistic method and TDS model. Second, the quantitative relationship between plastic deformation and hydrogen diffusion is established. At last, both qualitative and quantitative analysis are used to unambiguously elucidate the root causes of the impact of plastic deformation on hydrogen diffusion from microstructures

2.0 EXPERIMENTAL

All experiments were carried out in the following order: SSRT, hydrogen charging, TDS and TEM. Details are as follows.

2.1 Material and specimens

As-received S30408 is 5 mm-thick plate in hot-rolled condition and chemical compositions are given in Table 1, which conforms to the requirements of Chinese standard GB/T 24511. Materials were machined into SSRT specimens shown in Figure 1 by low-speed wire cutting machine. After polished to 2000 grit by silicon carbide abrasive paper, specimens were cleaned by ultrasonic cleaning using anhydrous ethanol to remove the residue of oil on surface.

Table 1 Chemical composition of S30408 austenite stainless steel (wt. %).

Chemical composition	C	Si	Mn	P	S	Cr	Ni	N
Experimental /wt. %	0.040	0.45	1.04	0.025	0.002	18.58	8.08	0.056
Standard /wt. %	≤0.08	≤0.75	≤2.00	≤0.035	≤0.020	18.00-20.00	8.00-10.50	≤0.10

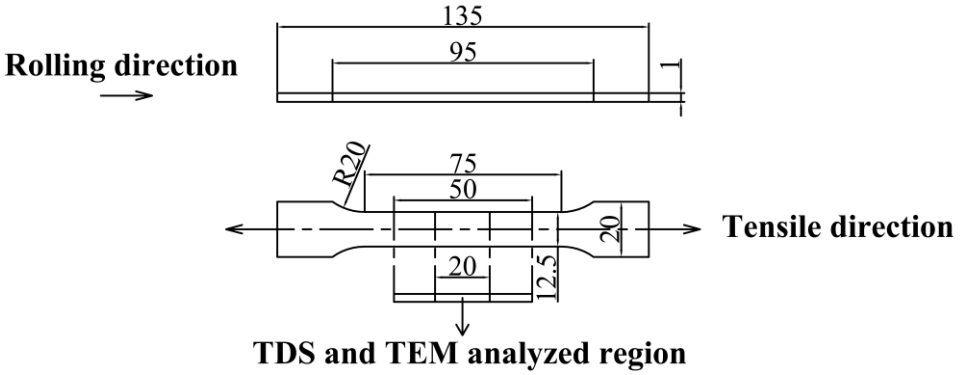

Figure 1. Specimens geometries of SSRT specimen and the sampling position of TDS and TEM (The dimensions are given in millimetre)

2.2 Slow Strain Rate Test

SSRT was conducted at room temperature with the crosshead rate of 0.05 mm·min^{-1}, corresponding to the strain rate of 1.1×10^{-5} /s. The applied strains were 4%, 6%, 8%, 10%, 12.5%, 17%, 18%, 19%, 20%, 21%, 22%, 23%, 28%, 32%, 36%, respectively. Plastic strain and volume fraction of strain-induced martensite (α'-martensite) were measured by extensometer and feritscope, respectively.

2.3 Hydrogen charging

Hydrogen was introduced into specimens after SSRT by means of high-temperature high-pressure gaseous hydrogen charging under the conditions of 453 K, 12 MPa for 80 h in GSH-2 autoclave.

2.4 Thermal Desorption Spectroscope

Temperature Programmed Desorption-workstation provided by Hiden Analytical Technology Ltd. was applied to attain hydrogen desorption spectroscope. Sampling position of TDS is shown in Figure 1 and TDS test was conducted after degassing and background when the pressure in the main chamber dropped into 5×10^{-9} torr to satisfy the accuracy requirement of mass spectrometer. Temperature rose from RT to 1000K at the ramp rate of 1 K/min which alleviated surface impedance lying behind anamorphose of experimental curves at a lower temperature.

2.5 Transmission Electron Microscopy

TEM images were obtained using FEI Tecnai G2 F20 S-TWIN instrument at room temperature with the acceleration voltage of 200 kV. Sampling position of TEM is shown in Figure 1 and TEM samples were prepared by twin-jet electropolishing technique. Electrolyte were prepared by mixing perchloric acid and ethanol with the volume ratio of 1:9 and the whole two jet course was conducted at -30℃ with 25mV and 8mA.

3.0 RESULTS AND DISCUSSION

3.1 Evolution of hydrogen diffusivities in deformed S30408

The variation of hydrogen diffusivities with plastic deformation is essential for the understanding of HE mechanism. In this section, an effective method is developed to deduce the apparent diffusivity of the deformed S30408. Based on the method, the relationship between plastic deformation and hydrogen diffusion is established quantitatively.

Hydrogen contents were attained from integration of hydrogen desorption rate after subtracted background and the results are shown in Figure 2. It can be seen that hydrogen contents vary from strain to strain with the same charging time. Specifically, hydrogen contents descend firstly and then ascend with the increment of plastic strain and appear linearly at a higher plastic strain. With the hydrogen charging condition mentioned above, hydrogen contents don't reach maximum value calculated by Sievert' law [31] and relevant parameters [31], so the higher hydrogen content in the specimens, the larger hydrogen diffusivities.

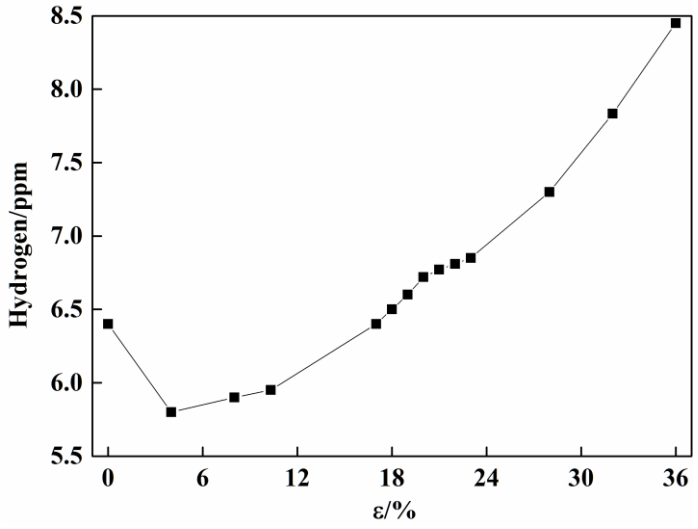

Figure 2. The variation of the hydrogen contents in the specimens with plastic strain

Based on TDS experiment results and TDS model, apparent diffusivities are calculated to establish the quantitative relationship between hydrogen diffusion and plastic deformation. Allow for a lower diffusivity of crystal lattice in S30408, TDS model adopted was built from the simplified diffusion equation and Oriani's assumption [13] which is a local equilibrium between hydrogen traps and crystal lattice. For slab sample, Ono and Meshii [37] have suggested the desorption rate are deduced as follows:

$$\frac{\partial C_{\mathrm{L}}}{\partial t}=-\left(\frac{\pi}{2d}\right)^{2} D_{\mathrm{e}}\left(C_{\mathrm{tot}}-C_{0}\right) \tag{1}$$

$$D_e = \frac{D_L}{1+\gamma C_T \exp\left(\frac{E_b}{RT}\right)} \tag{2}$$

$$C_{tot} = C_L + C_x = C_L\left[1+\gamma C_T \exp\left(\frac{E_b}{RT}\right)\right] \tag{3}$$

$$D_L = D_{0L}\exp\left(\frac{-E_{diff}}{RT}\right) \tag{4}$$

Taking into account the complexity of the effects of various hydrogen traps on hydrogen diffusion, crystal lattice together along with various hydrogen traps is perceived as a whole for simplicity and the effect of pre-existing traps on diffusion is reflected from the active energy of diffusion and prefactor of diffusion in Equation (4). For simplification, there are two ways to fit TDS peak. The first applies the same prefactor of diffusion and changes the activation energies of diffusion. The second applies the same activation of diffusion energy but different prefactors of diffusion. In this paper, the second method is chosen. Experiment curve with 0% strain can be fitted well with D_{oL} of 6.5×10^{-6} m^2/s and E_{diff} of 52800 J/mol shown in Figure 3(a). The other TDS curves are fitted with the same value of E_{diff} as 0% strain and different D_{oL}. By trial and error, the optimum parameters can be found eventually to fit corresponding experiment curves. The experiment and simulation results with or without strain and the parameters used for fitting experiment curves are given in Figure 3 and Table 2, respectively.

Hydrogen apparent diffusivities can be deduced through Equation (4) using the values of E_{diff} and D_{oL} listed at Table 2 and the results are shown in Figure 4. It can be seen that apparent diffusivity decreases firstly and then increases with the increment of plastic strain, which have the same tendency as hydrogen contents shown in Figure 2. Specifically, the results indicate that apparent diffusivities are smaller than that of 0% strain when plastic strains are below 20% but more than that of 0% strain when plastic strains are above 20%. In addition, one can conclude from that 20% strain acts as a turning strain of the effect of plastic deformation on hydrogen diffusivities. Based on it, the variation of hydrogen diffusivities is suggested to be divided into the two stages. In the first stage, hydrogen diffusion is inhibited when plastic deformation is approximately lower than 20% strain. In the second stage, it is promoted when plastic deformation is approximately higher than 20% strain.

Table 2 The fitting parameters used in TDS simulation with different strains.

Strain/%	0	4	8	10	12.5	20	32	36
$D_{0L}/10^{-6}$ m^2/s	6.500	1.968	2.020	3.272	3.443	5.304	22.000	28.400

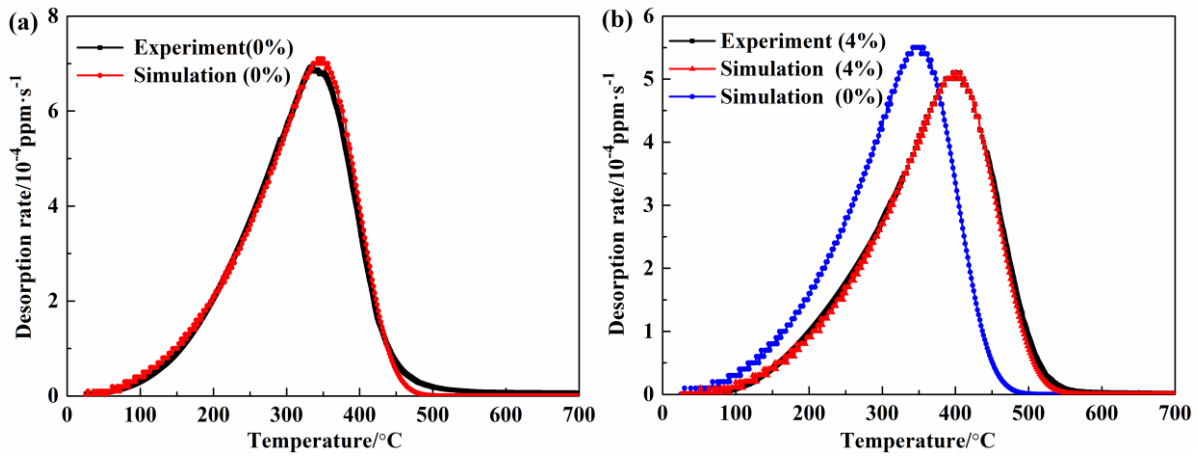

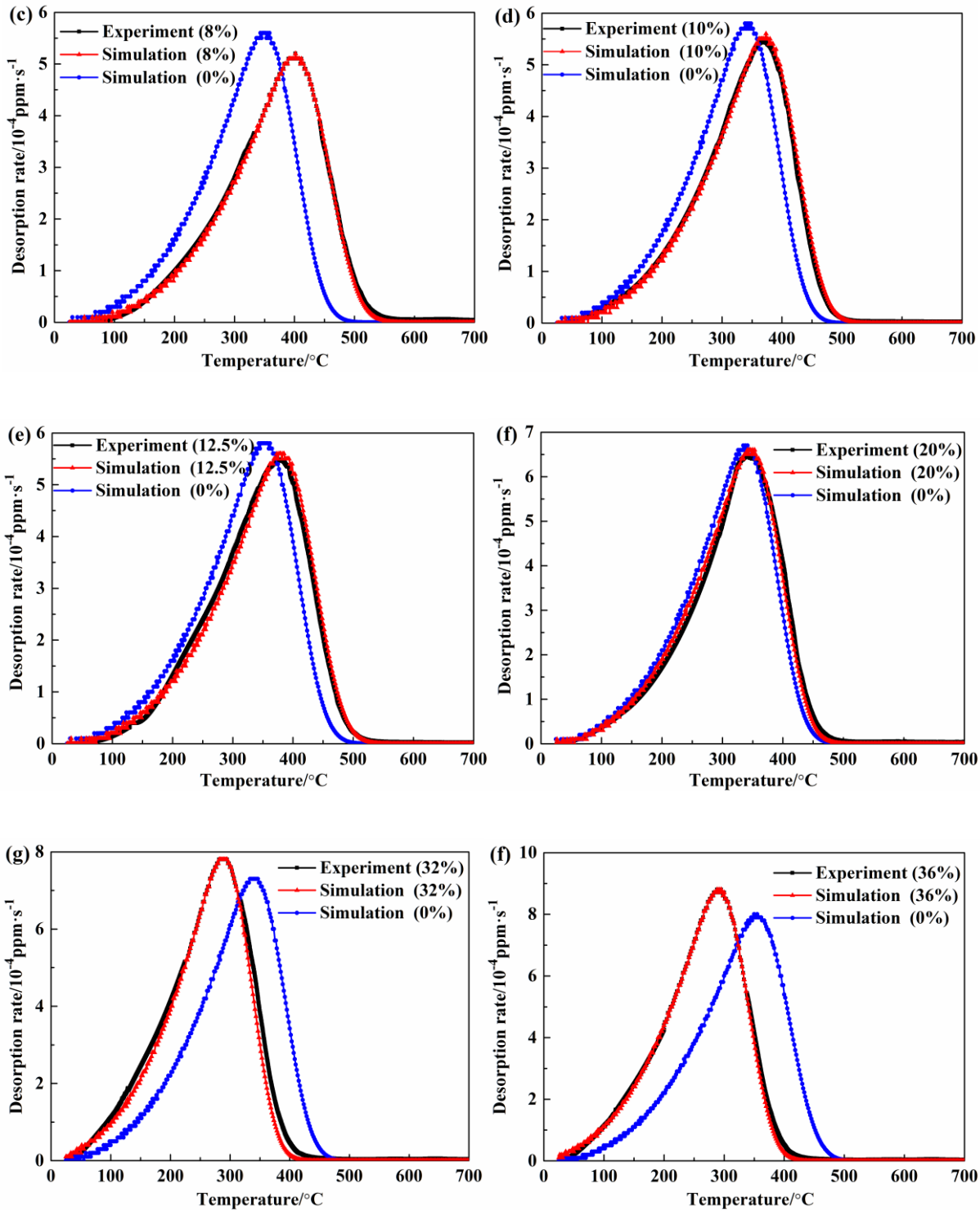

Figure 3. TDS experiment and simulation results with different plastic strain (a) 0%, (b) 4%, (c) 8%, (d) 10%, (e) 12.5%, (f) 20%, (g) 32%, (h) 36% (The blue curves are fitted with D_{oL} and E_{diff} of 0% strain)

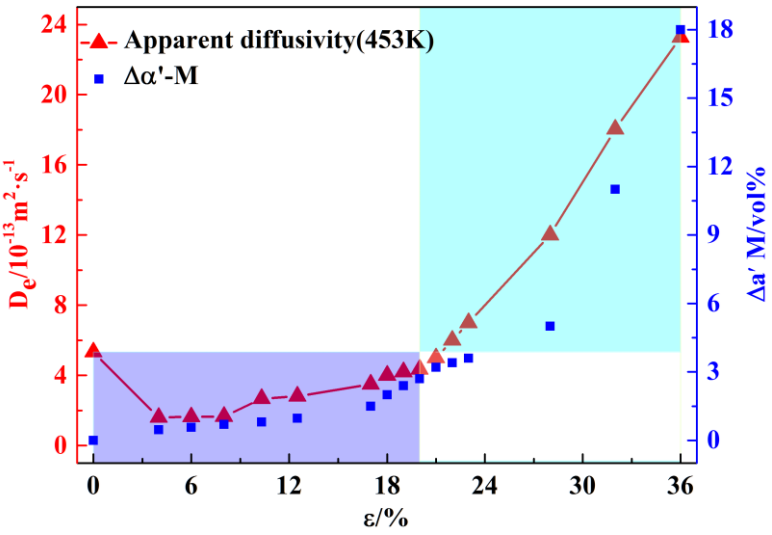

Figure 4. Hydrogen apparent diffusivities at 453 K changing with the plastic strain

3.2 Impact of microstructures on hydrogen diffusion

In addition to crystal lattice, hydrogen can also be captured by dislocation, grain boundary, phase interface, etc. In this section, it is discussed to explore the root cause of the impact of plastic deformation on hydrogen diffusion from microstructures.

It is well known that strain-induced martensite can be transformed from austenite in deformed S30408. In oder to quantify the amount of strain-induced martensite, the feritscope is used to detect volume fraction of strain-induced martensite which is magnetic while austenite is not. Results shown in Figure 5 are displayed via multi-measurement average and error bar. Measurement errors mostly focus on the range from 2% to 10%, implying an excellent performance in concentrating at mean values. From Figure 5, It can been seen that the amount of strain-induced martensite appears exponentially with the increase of plastic strain on the whole, which means plastic deformation plays a positive role in the formation of strain-induced martensite. Concretely speaking, the amount of α'-martensite induced by plastic deformation is smaller and increases slower during the initial stage of plastic deformation, while it becomes much more and faster with a larger plastic deformation. The amount of α'-martensite induced by plastic deformation in S30408 at 1.1×10^{-5} /s strain rate and room temperature are available as Equation (5):

$$\Delta\alpha' M(vol\%) = -0.10+0.27\exp(\varepsilon/8.71) \quad (5)$$

As shown in Figure 5, the amount of strain-induced martensite measured before and after hydrogen charging are almost overlap, which indicates that strain-induced martensite existing in S30408 has a high stability in 453 K and 12 MPa hydrogen for a long time. In other words, strain-induced martensite in S30408 does not disappear or aggrandize without stress field when it is subjected to the condition of hydrogen charging. Therefore, scilicet stress field is the necessary condition to form α'-martensite in S30408 while high temperature or high pressure are not.

For austenitic stainless steel, α'-martensite serves as a rapid path for hydrogen diffusion owing to the considerably difference of diffusivity and solubility between α'-martensite and austenite. Therefore, hydrogen is apt to diffuse through α'-martensite compared to austenite. Compared with Figure 4 and 5, the amount of strain-induced martensite is not completely consistent with hydrogen apparent diffusivities when the plastic strain is low, which means strain-induced martensite is not the only reason that affects hydrogen diffusion. In order to elucidate the root cause of the effect of plastic

deformation on hydrogen diffusion, TEM is used to understand microstructures changes at each stage other than strain-induced martensite and results are shown as Figure 6.

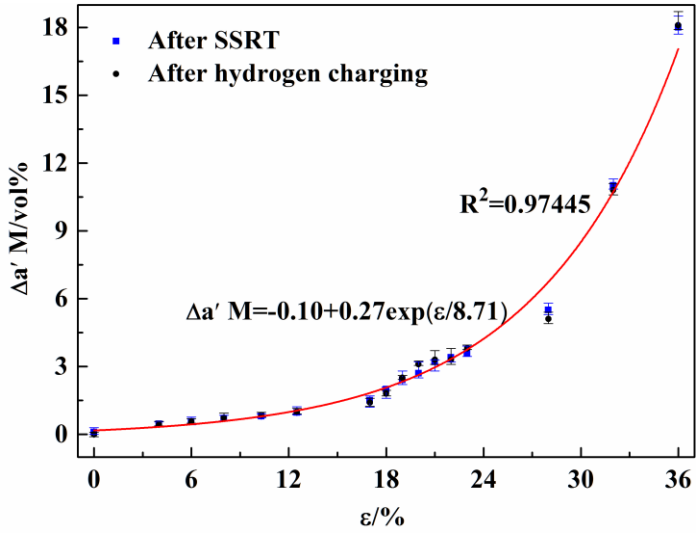

Figure 5. The transformation of strain-induced martnesite with plastic strain at room temperature and 1.1×10^{-5} /s strain rate

Figure 6 (a) shows dislocation of hydrogen-charged S30408 strained to 8%. A number of dislocations as well as bits of grain boundaries are present. Figure 6 (a) also indicates that almost no strain-induced martensite forms at 8% strain, which is consistent with the results shown as Figure 5. Therefore, in the first stage, plastic strain serves as a driving force of dislocation nucleation and proliferation and dislocation density increases with plastic deformation. Dislocation is quite counterproductive to hydrogen diffusion because of the difference between E_a and E_{diff}. E_a is given as the sum of E_b and E_t [38]. In practice, E_t is approximately equal to E_{diff} [39]. Therefore, E_a of dislocation is more than E_{diff}. Simultaneously, a smaller amount of strain-induced martensite is not by enough to promote hydrogen diffusion compared with the inhibitory effect of dislocation. Consequently, the inhibitory effect of dislocation surpasses the auxo-action of strain-induced martensite and becomes dominant for hydrogen diffusion.

Figure 6 (b) and magnified portions in Figure 6 (c) and (d) show an area fairly advanced in straining and it can be seen a rapid path for hydrogen diffusion is formed in S30408 strained to 36%. Figure 6 (c) and (d) are magnified views around the rapid path and indicate high-density dislocations are intertwined with strain-induced martensite, along with some grain boundaries in S30408 strained to 36%. Therefore, as the plastic deformation increases, dislocation pile-ups form and strain-induced martensite is inoculated from γ-austenite, ε-martensite and dislocation pile-ups. In addition to the increase in the amount of strain-induced martensite, distribution and morphology of it also play an important role in hydrogen diffusion. When the amount of strain-induced martensite reaches a certain value strain-induced martensite connects with each other and experiences the variation of morphology from point to sheet seen from Figure 6 (b). It implies an effective diffusion path in austenite is created and hydrogen diffusivities are improved apparently as a result. From Figure 4, apparent diffusivities have the same trend as the amount of strain-induced martnesite shown as Figure 5 when plastic strain exceeds 20%. Therefore, the auxo-action of strain-induced martensite becomes dominant for hydrogen diffusion insteading of dislocation at the second stage.

From above, we can seen that the influence of microstructure evolution on hydrogen diffusion of S30408 is a complicated process which involves multiple factors. Hydrogen diffusion cannot be predicted by single factor entirely or explained by one theory of HE perfectly for S30408. Overall, the

effect of plastic deformation at room temperature on hydrogen diffusion can be divided into two processes by about 20% strain. The first is dislocation controlling process and the second is controlled by strain-induced martensite.

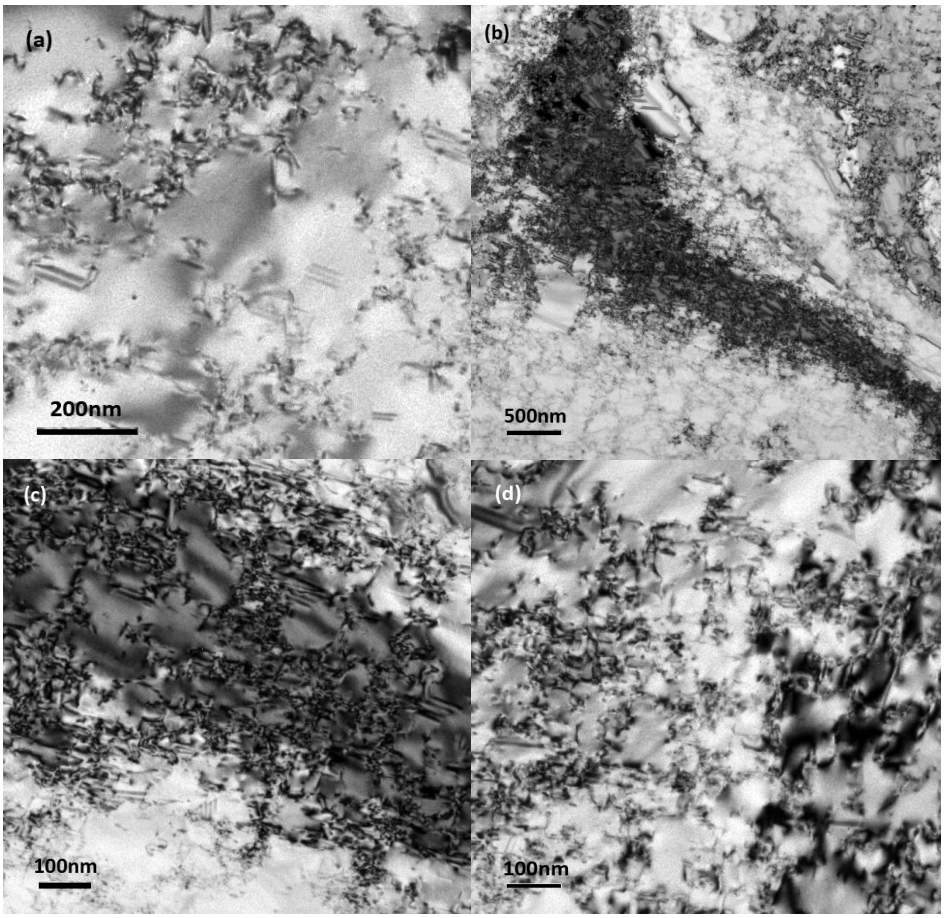

Figure 6. TEM micrographs of hydrogen-charged S30408 strained to 8% and 36% (a) dislocations in S30408 strained to 8%; (b) a rapid path for hydrogen diffusion in S30408 strained to 36%; (c) dislocations intertwined with strain-induced martensite in S30408 strained to 36%; (d) high-density dislocations in S30408 strained to 36%

4.0 CONCLUSION

In this paper, the quantitative relationship between apparent diffusivity and plastic strain has been built for further study of hydrogen diffusion and the mechanism of HE for S30408. Apart from it, this paper also focuses on the effect of pre-existing traps on hydrogen diffusion from microstructures. Main conclusions are as follows:

(1) There is a non-monotonic relation between hydrogen diffusivity and plastic strain. Apparent diffusivity of hot-rolled S30408 decreases firstly, and then increases with increasing plastic strain at room temperature. The transformation strain is about 20% demonstrated by experiments.

(2) Plastic deformation promotes the formation of α'-martensite. The effect of plastic deformation at room temperature on the transformation of the strain-induced martensite appears exponentially in hot-rolled S30408.

(3) The influence of microstructures on hydrogen diffusion of S30408 is a complicated process involving multiple factors. Hydrogen diffusion affected by plastic deformation is suggested to be divided into two processes by about 20% strain controlled by dislocations and strain-induced martensite, respectively.

ACKNOWLEDGMENTS

This research is supported by the Key Project of National Programs for Fundamental Research and Development (973 Program) of China (Number: 2015CB057601). The authors gratefully appreciate team members for their support and fruitful discussion for this study.

REFERENCES

[1] Jewett R.P., Walter R.J., Chandler W.T., Frohmberg R.P. Hydrogen Environment Embrittlement of Metals, 1973, NASA, Washington.

[2] Thompson A.W., Bernstein I.M. The Role of Metallurgical Variables in Hydrogen-Assisted Environmental Fracture (Fontana M.G., and Staehle R.W. Eds.), Springer, New York, 1980, p. 53.

[3] Briottet L., Moro I., Lemoine P., Quantifying the Hydrogen Embrittlement of Pipeline Steels for Safety Considerations, *International Journal of Hydrogen Energy*, **37**. No. 22, 2012, pp. 17616-17623.

[4] Sun X., Jian X., Li Y., Hydrogen Permeation Behaviour in Austenitic Stainless Steels, *Materials Science & Engineering A*, **114**. 1989, pp. 179-187.

[5] Tsong-Pyng P., Altstetter C.J., Effect of Deformation on Hydrogen Permeation in Austenitic Stainless Steels, *Acta Metallurgica*, **34**. No. 9, 1986, pp. 1771-1781.

[6] Gromov A.I., Kovneristyi Y.K., Permeability, Diffusion, and Solubility of Hydrogen in Cr-Ni and Cr-Mn Austenitic Steels, *Metal Science and Heat Treatment*, **22**. No. 5, 1980, pp. 321-324.

[7] Mitchell D.J., Edge E.M., Permeation Characteristics of Some Iron and Nickel Based Alloys, *Journal of Applied Physics*, **57**. No. 12, 1985, pp. 5226-5235.

[8] Grant D.M., Cummings D.L., Blackburn D.A., Hydrogen in 304 Steel: Diffusion, Permeation and Surface Reaction, *Journal of Nuclear Materials*, **149**. No. 2, 1987, pp. 180-191.

[9] Kishimoto N., Tanabe T., Suzuki T., Yoshida H., Hydrogen Diffusion and Solution at High Temperatures in 316l Stainless Steel and Nickel-Base Heat-Resistant Alloys, *Journal of Nuclear Materials*, **127**. No. 1, 1985, pp. 1-9.

[10] Grant D.M., Cummings D.L., Blackburn D.A., Hydrogen in 316 Steel - Diffusion, Permeation and Surface Reaction, *Journal of Nuclear Materials*, **152**. No. 2-3, 1988, pp. 139-145.

[11] Louthan Jr M., Derrick R., Donovan J., Hydrogen Transport in Iron and Steel. Effect of Hydrogen on Behavior of Materials; Proceedings of the International Conference, Wyoming, Metallurgical Society of AIME, Paper 337, 1976.

[12] And C.A.W., Frank R.C., Trapping of Interstitials in Metals, *Annual Review of Materials Research*, **13**. No. 1, 1983, pp. 139-172.

[13] Oriani R.A., The Diffusion and Trapping of Hydrogen in Steel, *Acta Metallurgica*, **18**. No. 1, 1970, pp. 147-157.

[14] Huang C.X., Yang G., Gao Y.L., Li S.D.W.S.X., Investigation on the Nucleation Mechanism of Deformation-Induced Martensite in an Austenitic Stainless Steel under Severe Plastic Deformation, *Journal of Materials Research*, **22**. No. 3, 2007, pp. 724-729.

[15] Das A., Sivaprasad S., Ghosh M., Chakraborti P.C., Tarafder S., Morphologies and Characteristics of Deformation Induced Martensite During Tensile Deformation of 304 Ln Stainless Steel, *Materials Science & Engineering A*, **486**. No. 1-2, 2008, pp. 283-286.

[16] Eliezer D., Chakrapani D.G., Altstetter C.J., Pugh E.N., The Influence of Austenite Stability on the Hydrogen Embrittlement and Stress-Corrosion Cracking of Stainless Steel, *Metallurgical and Materials Transactions A*, **10**. No. 7, 1979, pp. 935-941.

[17] Liu R., Narita N., Altstetter C., Birnbaum H., Pugh E.N., Studies of the Orientations of Fracture Surfaces Produced in Austenitic Stainless Steels by Stress-Corrosion Cracking and Hydrogen Embrittlement, *Metallurgical and Materials Transactions A*, **11**. No. 9, 1980, pp. 1563-1574.

[18] Vennett R.M., Ansell G.S., The Effect of High-Pressure Hydrogen Upon the Tensile Properties and Fracture Behavior of 304l Stainless Steel, *ASM-Trans*, **60**. 1967, pp. 242-251.

[19] Bentley A.P., Smith G.C., Effect of Prior Cold Work on Hydrogen-Induced Surface Cracking in Austenitic Stainless Steels, *Scripta Metallurgica*, **20**. No. 5, 1986, pp. 729-732.

[20] Hedström P., Lienert U., Almer J., Odén M., Stepwise Transformation Behavior of the Strain-Induced Martensitic Transformation in a Metastable Stainless Steel, *Scripta Materialia*, **56**. No. 3, 2007, pp. 213-216.

[21] Ladna B., Birnbaum H., A Study of Hydrogen Transport During Plastic Deformation, *Acta Metallurgica*, **35**. No. 7, 1987, pp. 1775-1778.

[22] Briant C.L., Hydrogen Assisted Cracking of Type 304 Stainless Steel, *Metallurgical and Materials Transactions A*, **10**. No. 2, 1979, pp. 181-189.

[23] Hänninen H., Hakarainen T., On the Effects of α' Martensite in Hydrogen Embrittlement of a Cathodically Charged Aisi Type 304 Austenitic Stainless Steel, *Corrosion*, **36**. No. 1, 1980, pp. 47-51.

[24] Fukuyama S., Imade M., Lin Z., Yokogawa K. Hydrogen Embrittlement of Metals in 70 Mpa Hydrogen at Room Temperature, 2005 ASME Pressure Vessels and Piping Division Conference, Denver, ASME, Paper 493, 2005.

[25] Fukuyama S., Imade M., Iijima T., Yokogawa K. Development of New Material Testing Apparatus in 230 Mpa Hydrogen and Evaluation of Hydrogen Gas Embrittlement of Metals, 2008 ASME Pressure Vessels and Piping Division Conference, Chicago, ASME, Paper 235, 2008.

[26] Matsunaga H., Noda H., Visualization of Hydrogen Diffusion in a Hydrogen-Enhanced Fatigue Crack Growth in Type 304 Stainless Steel, *Metallurgical and Materials Transactions A*, **42**. No. 9, 2011, pp. 2696-2705.

[27] Rozenak P., Stress Induce Martensitic Transformations in Hydrogen Embrittlement of Austenitic Stainless Steels, *Metallurgical and Materials Transactions A*, **45A**. No. 1, 2014, pp. 162-178.

[28] Tien J., Thompson A.W., Bernstein I.M., Richards R.J., Hydrogen Transport by Dislocations, *Metallurgical and Materials Transactions A*, **7**. No. 6, 1976, pp. 821-829.

[29] Kurkela M., Frankel G.S., Latanision R.M., Suresh S., Ritchie R.O., Influence of Plastic Deformation on Hydrogen Transport in 2 Ja:Math Cr-1mo Steel, *Scripta Metallurgica*, **16**. No. 4, 1982, pp. 455-459.

[30] Donovan J.A., Sorption of Tritium by Nickel During Plastic Deformation, *Metallurgical and Materials Transactions A*, **7**. No. 1, 1976, pp. 145-149.

[31] Marchi C.S., Somerday B.P., Robinson S.L., Permeability, Solubility and Diffusivity of Hydrogen Isotopes in Stainless Steels at High Gas Pressures, *International Journal of Hydrogen Energy*, **32**. No. 1, 2007, pp. 100-116.

[32] Banerjee K., Chatterjee U.K., Hydrogen Permeation and Hydrogen Content Under Cathodic Charging in Hsla 80 and Hsla 100 Steels, *Scripta Materialia*, **44**. No. 2, 2001, pp. 213-216.

[33] Hadam U., Zakroczymski T., Absorption of Hydrogen in Tensile Strained Iron and High-Carbon Steel Studied by Electrochemical Permeation and Desorption Techniques, *International Journal of Hydrogen Energy*, **34**. No. 5, 2009, pp. 2449-2459.

[34] Frappart S., Feaugas X., Creus J., Thebault F., Delattre L., Marchebois H., Study of the Hydrogen Diffusion and Segregation into Fe-C-Mo Martensitic Hsla Steel Using Electrochemical Permeation Test, *Journal of Physics & Chemistry of Solids*, **71**. No. 10, 2010, pp. 1467-1479.

[35] Rozenak P., Bergman R., X-Ray Phase Analysis of Martensitic Transformations in Austenitic Stainless Steels Electrochemically Charged with Hydrogen, *Materials Science & Engineering A*, **437**. No. 2, 2006, pp. 366-378.

[36] Harris D., Pickering H. On Anodic Cracking During Cathodic Hydrogen Charging, Technical Report No. ADA018286.

[37] Ono K., Meshii M., Hydrogen Detrapping from Grain Boundaries and Dislocations in High Purity Iron, *Acta Metallurgica Et Materialia*, **40**. No. 6, 1992, pp. 1357-1364.

[38] Dietzel W., Atrens A., Barnoush A. Gaseous Hydrogen Embrittlement of Materials in Energy Technologies, 2012, Woodhead Publishing, UK.

[39] Wei F.G., Hara T., Tsuzaki K., Precise Determination of the Activation Energy for Desorption of Hydrogen in Two Ti-Added Steels by a Single Thermal-Desorption Spectrum, *Metallurgical & Materials Transactions B*, **35**. No. 35, 2004, pp. 587-597.